REVIEW OF THE STRUCTURE OF HADRONS FROM LEPTON-NUCLEON INTERACTIONS

J. Drees

Fachbereich Physik
Universität-Gesamthochschule Wuppertal
Wuppertal, Fed. Rep. Germany

1. INTRODUCTION

During the last years a central aspect of deep inelastic lepton nucleon scattering has been the collection of high precision data sets needed for a thorough confrontation with predictions from quantum chromodynamics. This, on the other hand, has become a tedious task. After the original excitement about scaling violations behaving exactly like vital QCD expectations, it has become clear that in the kinematical region where we have data, there are additional phenomena at work besides perturbative QCD. Consequently the analysis of the data has become more and more sophisticated, and only slowly - maybe within the last few months - there seems to be a new convergence. However, there are still some problematic or unsatisfactory points. The situation with respect to the neutrino total cross sections has been discussed by Wotschack[1]. I will start with a discussion of the measurements of the ratio of longitudinal to transverse absorption cross sections. The two main parts of my talk will then deal with our present knowledge of the parton constituency of the nucleon and a discussion of QCD fits including the separation of higher twist parts.

Some aspects only briefly summarized in this talk have been discussed in more detail in reviews presented at previous conferences[2)3)].

2. WHAT DO WE KNOW ABOUT R ?

The determination of the ratio of longitudinal to transverse absorption cross sections

$$R \equiv \sigma_L/\sigma_T = (F_2\ (1 + Q^2/\nu^2) - 2\ x\ F_1)\ /\ 2\ xF_1$$

or equivalently

$$R' \equiv F_L/F_2 = (F_2 - 2\ xF_1)\ /\ F_2 \qquad (< R)$$

is important for the following reasons:

1. R contains information about the spin of the constituents of the nucleon contributing to the interaction.

2. In QCD one expects

$$R \propto \alpha_s\ (Q^2).$$

More specifically, in leading order[4)]

$$F_L(x,Q^2) = \frac{\alpha_s(Q^2)}{2\pi}\ x^2 \int_x^1 \frac{dy}{y^3} \left[\frac{8}{3}\ F_2(y,Q^2) + 4\ a\ (1 - \frac{x}{y})\ y\ G(y,Q^2)\right]$$

with $a = 4$ for neutrino scattering and $a = \frac{10}{9}$ for muon scattering (assuming 4 quark flavours). The first term contributes mainly at large x ($x > .2$), the second term dominates at small x ($x < .1$). Thus good data on R would allow either a direct estimate of the effective strong interaction coupling α_s or of the gluon distribution $G(x,Q^2)$.

Unfortunately a measurement of $R(x,Q^2)$ is very hard since one has to compare absolutely normalized cross sections measured at fixed x,Q^2 but different primary lepton energies. Still, some knowledge of R is essential, because

3. the determination of F_2 from the experimental double differential cross section depends on R. Especially the variation of F_2 with Q^2 at fixed x is sensitively affected,[5]

$$F_2 = \frac{\frac{1}{\sigma_0}\frac{d^2\sigma}{dx\,dy}}{1 + (1-y)^2 - y^2 R'} \qquad \text{with} \qquad y = \frac{Q^2}{2MxE} .$$

Consequently, many groups have presented average values of R (or R') and some groups have even measured R as a function of x or Q^2. Fig. 1 shows recent results from the CDHS collaboration[6] together with typical QCD predictions for Λ = 500 and 200 MeV[7]. Both statistical plus systematical errors are indicated.

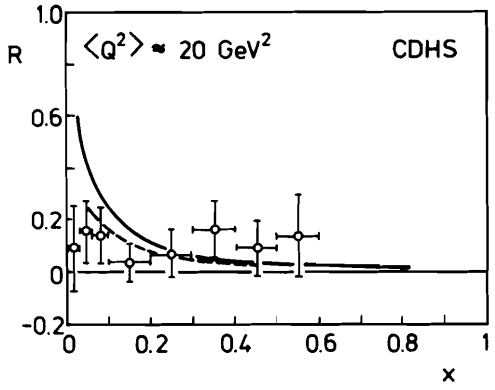

Fig. 1

R values from νN scattering. The curves indicate QCD predictions for Λ = 500 MeV (solid curve) and Λ = 200 MeV (dotted curve).

R seems to be independent of x, furthermore no significant dependence on Q^2 is found. There is no exciting agreement with the QCD curves, but since the experimental errors are large no firm conclusion is possible.

Fig. 2 presents a summary of R data from charged lepton-proton scattering. The error bars include both statistical and systematical uncertainties.

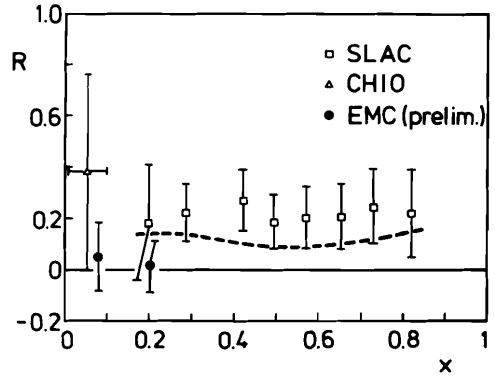

Fig. 2

R values from e,μp scattering. The Q^2 range of the SLAC data is $1 \leq Q^2 \leq 4$ GeV^2 at x = 0.2 and $12 \leq Q^2 \leq 18$ GeV^2 at x = 0.8. The curve presents a prediction for QCD plus diquark scattering[10].

There is no indication of a x dependence in the SLAC data[8)9)]. The point from the CHIO collaboration[11)] represents their average value for $x > 0.01$. For very small $x < 0.01$ the CHIO group finds $R = 1.22 + .61 - .67$. Also shown are two preliminary values from the EMC[12)] at $x = .08$, $\langle Q^2 \rangle = 12$ GeV^2, and $x = .2$, $\langle Q^2 \rangle = 30$ GeV^2.

Larger values of R at large x could be caused by a contribution of integer spin objects to the scattering process. Abbott et al.[10)] have considered the effect of a significant dynamical diquark substructure in the nucleon, i.e. higher twist effects of order $1/Q^2$ and $1/Q^4$. The dashed curve in Fig. 2 shows the prediction for QCD plus diquark scattering calculated by using the average value Q^2 of the SLAC data in each x bin. The prediction reflects roughly the shape of the data.

The CDHS and EMC measurements have higher $\langle Q^2 \rangle$. Thus higher twist effects are expected to be smaller, a trend consistent with the data.

A summary of average values of R or R' obtained by various groups is collected in Table 1 including results from neutrino groups having explicitely evaluated the radiative corrections to their data (which change somewhat the shape of the y distribution).

Table 1 Average values of R or R'

Experiment		Reaction	R	R'
SLAC[9)]	'78	ep	0.21 ± 0.10	
SLAC-MIT[8)]	'79	ed	0.17 ± 0.07	
CHIO (x>.01)[11)]	'80	μp	0.38 ± 0.38	
EMC[12)] prelim.	'81	μp	0.03 ± 0.10	
		μFe	-0.13 ± 0.19	
HPWFOR[13)]	'79	νN		0.18 ± 0.07
CDHS[6)]	'81	νN	0.10 ± 0.07	
BEBC[14)]	'81	νN		0.04 ± 0.16
FIIM (FNAL 15')[15)]	'81	νN		0.03 ± 0.12
CHARM[16)]	'81	N.C.		0.10 ± 0.10

It is hard to draw any firm conclusion from these values, but perhaps one can say: There is a tendency toward small positive values of R. The more recent experiments seem to indicate even smaller values than those measured by SLAC at lower beam energies.

3. THE PARTON CONSTITUENCY OF THE NUCLEON

As well known the relations between structure functions and quark distribution functions as given by the quark parton model remain unchanged in leading order QCD except that all quark distributions evolve with Q^2 in the characteristic manner described by the Altarelli-Parisi equations[17)], e.g.

$$xF_3 \equiv \frac{1}{2}\,(x\,F_3^{\nu N} + x\,F_3^{\bar{\nu}N}) = x\,(q - \bar{q})$$

$$F_2^{\nu N} = x\,(q + \bar{q})$$

$$F_2^{\mu N} = \frac{5}{18}\,x\,(q + \bar{q}) - \frac{1}{6}\,x\,(s + \bar{s} - c - \bar{c})$$

where

$$q(x,Q^2) = u(x,Q^2) + d(x,Q^2) + s(x,Q^2) + c(x,Q^2)$$

etc.

The progress achieved during the last year comes from the experimental side. Table 2 summarizes the experiments contributing new or improved data.

Table 2 New data on structure functions 1981

Experiment	Reaction	Quantities	x range	Q^2 range GeV^2
GGM[18]	$\nu,\bar{\nu}N$	xF_3, $F_2^{\nu N}$	0 - 0.8	0.5 - 50
BEBC I[14]	$\nu,\bar{\nu}N$	xF_3, $F_2^{\nu N}$	0 - 1.	0.01 - 100
BEBC II[19]	$\bar{\nu}d,\nu d$	$u,\bar{d} + \bar{s},\ldots$		
CHARM[20]	$\nu,\bar{\nu}N$	xF_3, $F_2^{\nu N}$	0 - 0.65	0.2 - 180
CDHS[21]	$\nu,\bar{\nu}N$	xF_3, $F_2^{\nu N}$,$\bar{q}$	0 - 0.7	1 - 280
CFRR[22]	$\nu,\bar{\nu}N$	xF_3, $F_2^{\nu N}$	0 - 0.7	4 - 25
FIIM[15]	$\bar{\nu}N$	$F_2^{\nu N}$, $xF_3^{\bar{\nu}N}$	0 - 1.	averaged
EMC[23]	μp,d	$F_2^{\mu p}$, $F_2^{\mu n}$	0.02 - 0.7	2 - 200
	μFe	$F_2^{\mu N}$		
BCDMS[24]	μC	$F_2^{\mu N}$	0.3 - 0.7	25 - 280

New F_2 Data from Heavy Targets.

The structure function F_2 is most precisely determined, both in muon and neutrino experiments. It is very instructive to compare the results of the various groups since there are differences in the analysis and the systematic errors. E.g. F_2 from muon experiments, because of the $1/Q^4$ propagator factor in the differential cross section, depends sensitively on a good knowledge of the incident and scattered muon momentum. Therefore, the momentum and trajectory of each incident muon is measured in the CERN experiments . Also radiative corrections may become large at large y and small x. For the data presented the correction is always less than 25%.

F_2 from neutrino experiments depends on calorimetry, on scattering angle determination, and possibly on normalization uncertainties.

The values of R assumed for the F_2 extraction are somewhat different for

the different experiments. EMC and BCDMS assume R = 0, CDHS assumes R = 0.1.

Figs. 3, 4 and 5 show fully analyzed heavy target measurements of $F_2^{\mu N}$ for $x \geq 0.25$ obtained by EMC[23b] and by BCDMS[24] at various beam energies and of $F_2^{\nu N}$ measured by CDHS[2] multiplied by 5/18 representing the average charge squared of the quarks inside the nucleon. In all cases no corrections for the Fermi motion and the binding of the nucleons are applied. There is excellent agreement between the new results from the various experiments within the statistical and systematical errors.

In the region of small x good agreement is observed between the CDHS and the EMC measurements. On the other hand, the preliminary values on $F_2^{\nu N}$ presented this year by the CFRR collaboration[22] are significantly above the CDHS results at $x < 0.2$, while both experiments agree at large x. Clearly it is important to resolve this problem.

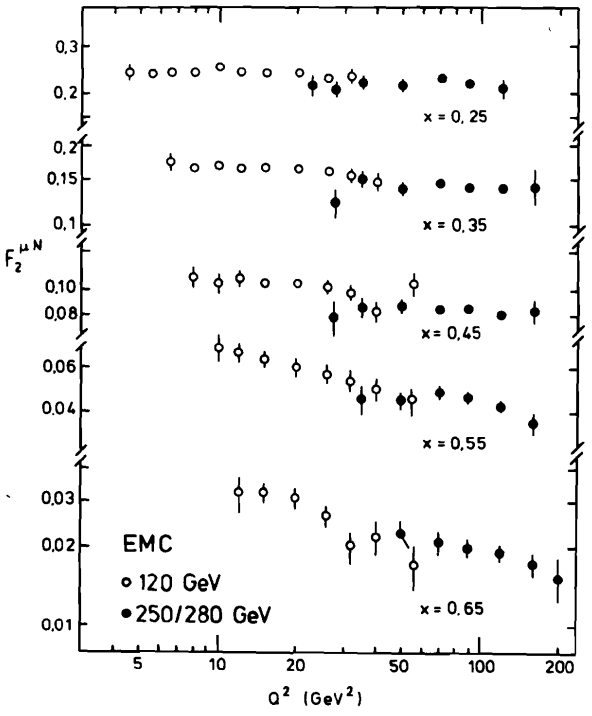

Fig. 3 $F_2^{\mu N}$ versus Q^2 for $x \geq 0.25$ from EMC measured with an iron target assuming R = 0.

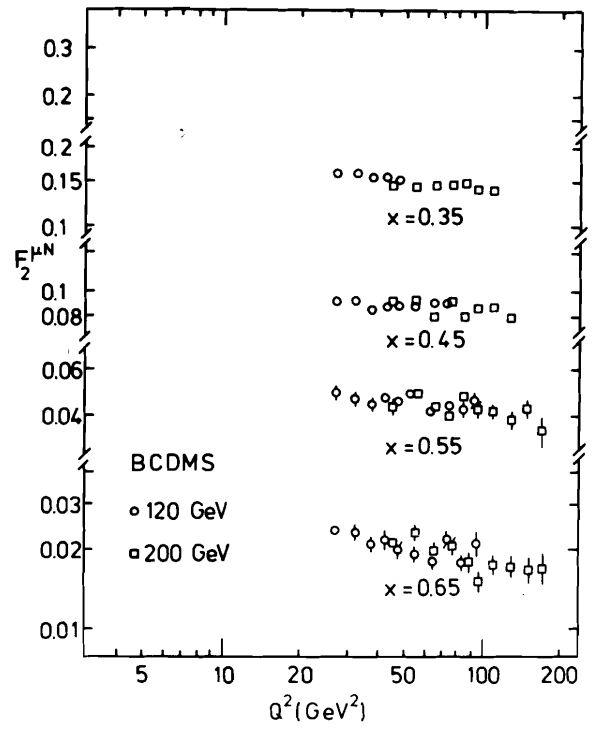

Fig. 4

$F_2^{\mu N}$ from BCDMS measured with a carbon target assuming R = 0.

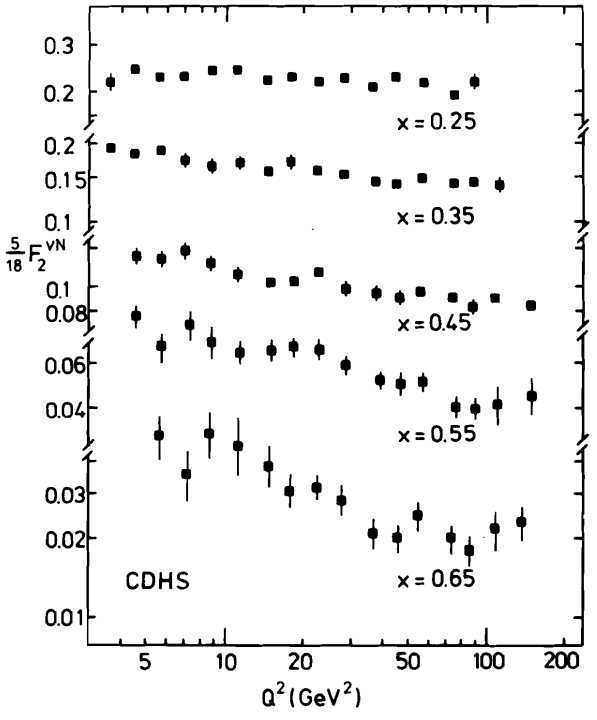

Fig. 5

5/18 $F_2^{\nu N}$ from CDHS measured with an iron target assuming R = 0.1.

The data clearly verify the familiar pattern of scaling violations, in particular the decrease with Q^2 at large x. However, there is some tendency that F_2 becomes flatter at fixed x with increasing Q^2. In principle, such an effect is expected by QCD, but the measurements indicate even smaller slopes $\partial F_2/\partial \ln Q^2$ than expected on the basis of an extrapolation from QCD fits to the earlier data at lower Q^2. I will discuss this point in chapter 4 in some detail.

A thorough comparison of F_2 data from various e and μ experiments can be found in the paper of Smadja[25].

u/d Ratios.

The first information on the ratio of d over u quark distribution functions was obtained from the ep and ed data of the SLAC-MIT group[26]. New results on $F_2^{\mu n}/F_2^{\mu p}$ ratios are reported by the EMC[27] at Q^2 between 10 and 90 GeV^2. Experimentally this quantity is well determined since several systematic errors tend to cancel in the cross section ratio. In the large x region (x > 0.2) where sea quarks can be neglected,

$$\frac{F_2^{\mu n}}{F_2^{\mu p}} = \frac{1 + 4\ d/u}{4 + d/u}$$

permitting a determination of the ratio d/u which can be confronted with several models.

Fig. 6 shows the preliminary EMC results obtained from hydrogen and deuterium runs at 280 GeV muon beam energy. At each x the data are integrated over Q^2. A comparison with the SLAC data[8] (covering a Q^2 region from about 1 to 20 GeV^2) yields good agreement. Clearly u quarks dominate at large x, for x = 0.65 the EMC finds about four times more u than d quarks.

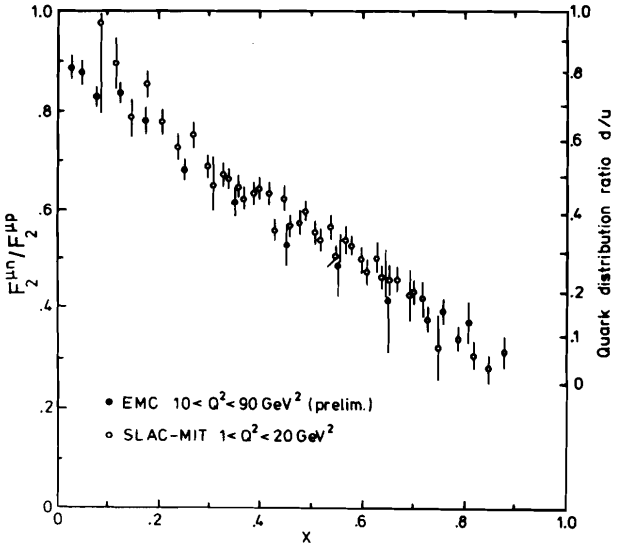

Fig. 6

$F_2^{\mu n}/F_2^{\mu p}$ or $F_2^{\mu n}/F_2^{\mu p}$ versus x integrated over the accessible range of Q^2. The scale on the right side shows the quark distribution ratio d/u. The EMC points are evaluated by using preliminary 280 GeV deuterium data together with 120 and 280 GeV hydrogen data.

Another method providing d/u ratios is based on the comparison of νp and e,μp cross sections. Since here only data from hydrogen targets are involved, problems arising from corrections due to the Fermi motion in the deuteron are avoided. At large x

$$\frac{F_2^{\nu p}}{F_2^{\mu p}} = \frac{18\ d/u}{4 + d/u} \ .$$

In Fig. 7 results obtained by a BEBC group[28] using their charged current νp data together with SLAC ep and EMC μp data are shown. Plotted is the quantity $1/4 + 5/24\ F_2^{\nu p}/F_2^{\mu p}$ which should be equal to $F_2^{\mu n}/F_2^{\mu p}$ in the region where valence quarks dominate. The Q^2 range extends from 2 to 70 GeV^2 for each x bin.

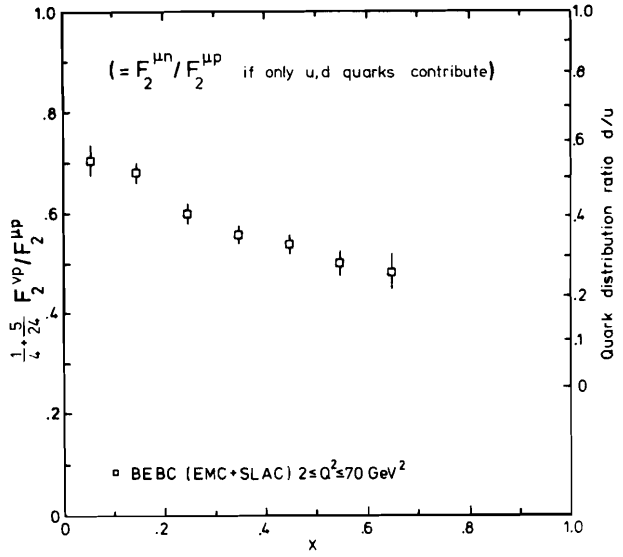

Fig. 7

$\frac{1}{4} + \frac{5}{24} F_2^{\nu p}/F_2^{\mu p}$ and the ratio of quark distributions d/u versus x.

One observes quite good agreement with $F_2^{\mu n}/F_2^{\mu p}$ for $0.4 \leq x \leq 0.7$. However, at small x the μn/μp ratios are above the corresponding νp/μp values. From the parton model one would expect $F_2^{\mu n}/F_2^{\mu p} > 1/4 + 5/24 \cdot F_2^{\nu p}/F_2^{\mu p}$ if $\bar{d} > u + 3/5\ s$ in the region where sea quark effects are important. Such a behaviour has been expected by Field and Feynman[29].

The Q^2 variation of the μn/μp and en/ep ratios are shown in Fig. 8 for various fixed x. QCD expects no strong variation over the accessible Q^2 region. For instance, from the parametrization of the parton distribution functions due to Glück, Hoffmann and Reya[30], one computes an increase of the n/p ratio of 1% at $x = 0.08$ and a decrease of 4% at $x = 0.65$ with Q^2 increasing from 5 to 90 GeV^2.

Diquark models, on the other hand, expect quite a sizable variation as shown by the solid curves in Fig. 8, representing a prediction of Donnachie and Landshoff[31]. Their model is build in such a way that the entire scaling violation observed for the SLAC hydrogen and deuterium data with $x > 0.3$ is explained by a Q^2 dependent diquark term behaving like $1/(1 + Q^2/M^2)$. It seems fair to conclude that this model leads to an overestimate of diquark effects.

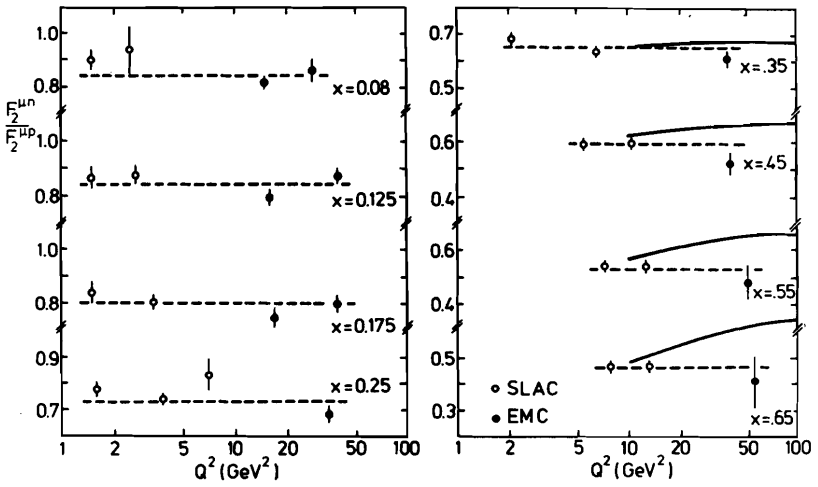

Fig. 8 $F_2^{\mu n}/F_2^{\mu p}$ (or en/ep) versus Q^2. The dashed lines indicate the weighted mean value at each x. The solid curves show predictions of a diquark model[31].

The strong dominance of u over d quarks at high x has also been confirmed by neutrino bubble chamber experiments measuring charged current $\nu n/\nu p$ and $\bar{\nu} n/\bar{\nu} p$ ratios[32)19)] or by comparing x distributions of νp and $\bar{\nu} p$ events[33]. Reviews of the results have been given by Wahl[2)] and by Wotschack[1)]. Therefore, I can confine myself to mentioning the new results contributed by a BEBC group[19)] analyzing 5630 $\bar{\nu}d$ and 1372 νd interactions. For the total cross section ratios they find,

$$\frac{\sigma(\bar{\nu}n)}{\sigma(\bar{\nu}p)} = 0.51 \pm 0.01\ (\pm\ 0.03), \qquad \frac{\sigma(\nu n)}{\sigma(\nu p)} = 2.22 \pm 0.12\ (\pm\ 0.25),$$

consistent with earlier measurements, but with substantially smaller errors for the antineutrino case (the second error is due to systematical uncertainties). Their results on the x dependence are given in Fig. 9a. At large x the ratio $d\sigma^{\bar{\nu}n}/dx$ over $d\sigma^{\bar{\nu}p}/dx$ directly measures the d/u ratio. In the accessible x region the data are well described by the Field, Feynman parton model[29)].

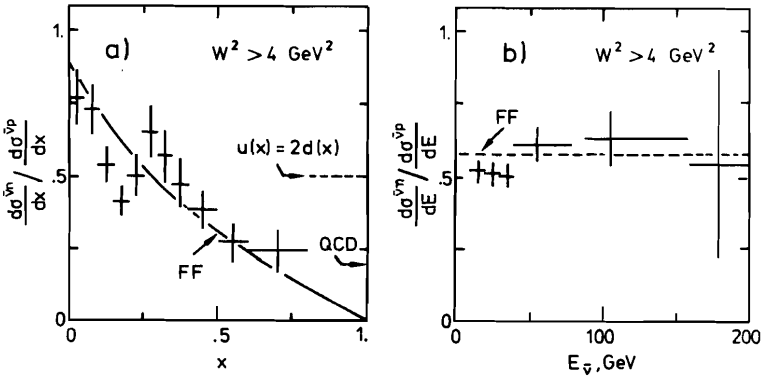

Fig. 9
a) $\frac{d\sigma^{\bar{\nu}n}}{dx} / \frac{d\sigma^{\bar{\nu}p}}{dx}$ versus x for $W^2 > 4$ GeV^2. The solid curve is computed by using the quark distribution functions of Field and Feynman.

b) $\frac{d\sigma^{\bar{\nu}n}}{dE} / \frac{d\sigma^{\bar{\nu}p}}{dE}$ versus $E_{\bar{\nu}}$.

As indicated in Fig. 9b), there is no significant variation of the $\bar{\nu}n/\bar{\nu}p$ ratio with the beam energy $E_{\bar{\nu}}$ or equivalently with $\langle Q^2 \rangle$.

Summarizing the results on d/u ratios we can conclude:

1. All experiments agree on the rapid fall of d/u with increasing x.
2. The dependence on Q^2 is weak in agreement with QCD expectations.
3. In the highest x bin available, all experiments find $d/u \lesssim 0.25$.

The Q^2 Evolution of Light Antiquarks.

High statistic neutrino experiments have the special advantage that they are able to measure the Q^2 variation of the light antiquark momentum distribution $x\bar{q}(x,Q^2) = x(\bar{u} + \bar{d} + 2\,\bar{s})$. At high y

$$x\bar{q}(x,Q^2) \simeq \frac{\pi}{G^2\,ME}\left(\frac{d^2\sigma^{\bar{\nu}N}}{dx\,dy} - (1-y)^2\,\frac{d^2\sigma^{\nu N}}{dx\,dy}\right) + \Delta$$

with Δ depending on $(1-y)^2 \cdot x(\bar{s} - \bar{c})$ and R'. Obviously one needs good measurements of the antineutrino cross section.

Recent progress comes from the CDHS analysis of 150 000 $\bar{\nu}N$ events from the wide band beam and of 25 000 $\bar{\nu}N$ from the narrow band beam[34]. The extracted antiquark distribution is shown in Fig. 10 as a function of Q^2 for various x bins.

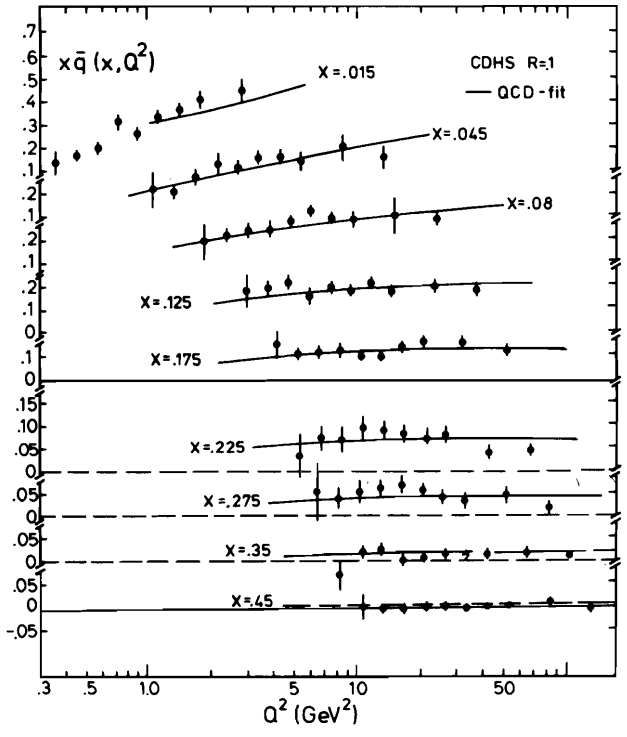

Fig. 10

Light antiquark distribution $x\bar{q}$ from CDHS. The curves represent a leading order QCD fit.

At small x a strong rise of $x\bar{q}$ with Q^2 is observed. Furthermore, it must be noted that the antiquark distribution extends to $x > 0.35$ and disappears for $x \gtrsim 0.45$. As an important consequence of this measurement it becomes now possible to analyze the Q^2 evolution of the gluon distribution.

The Momentum Distribution of Gluons.

Knowing the antiquark momentum distribution $x\bar{q}\,(x,Q^2)$ and $F_2\,(x,Q^2)$, the Q^2 evolution of the gluon distribution can be directly evaluated from the Altarelli-Parisi equations:

$$\frac{\partial \bar{q}(x,Q^2)}{\partial \ln Q^2} = \frac{\alpha_s(Q^2)}{2\pi} \int_x^1 \frac{dy}{y} \left[\bar{q}(y,Q^2)\, P_{q\leftarrow q}\left(\frac{x}{y}\right) + N_f\, G(y,Q^2)\, P_{q\leftarrow g}\left(\frac{x}{y}\right) \right]$$

$$\frac{\partial F_2(x,Q^2)}{\partial \ln Q^2} = \frac{\alpha_s(Q^2)}{2\pi} \int_x^1 x\frac{dy}{y^2} \left[F_2(y,Q^2)\, P_{q\leftarrow q}\left(\frac{x}{y}\right) + 2 N_f\, y\, G(y,Q^2)\, P_{q\leftarrow g}\left(\frac{x}{y}\right) \right]$$

The functions $P_{q\leftarrow q}$ respectively $P_{q\leftarrow g}$ describe the splitting of a quark into a quark and a gluon respectively of a gluon into a quark-antiquark pair and are well known from perturbation theory.

An analysis along this line was performed by the CDHS group[34]. The sensitive tool is the logarithmic slope of the antiquark distribution which is mainly connected to the splitting of a gluon into a quark-antiquark pair while both processes contribute about equally to the Q^2 evolution of F_2.

The results of a leading order QCD fit to both $x\bar{q}$ and F_2 using a technique of Abbott and Barnett[35] is presented in Fig. 11 for $Q^2 = 4.5$ and $22.5\ \mathrm{GeV}^2$. A cut was made to the data so that $W^2 > 11\ \mathrm{GeV}^2$ in order to reduce to some extent higher twist contributions. The fit included target mass effects and enforced energy momentum conservation for the sum of all partons, some results are:

$$\left.\begin{aligned} \Lambda &= 180 \pm 20\ \mathrm{MeV} \\ \langle F_2 \rangle &= 0.45 \\ \langle x\bar{q} \rangle &= 0.055 \end{aligned}\right\} \text{ at } Q_o^2 = 5\ \mathrm{GeV}^2 ,$$

i.e. about 55% of the nucleon momentum is carried by gluons.

It is important to notice that the shape of the gluon distribution changes strongly with Q^2. No acceptable fit is possible if the gluon distribution is parametrized in the simple form $x\,G(x,Q^2) \propto (1-x)^{P(Q^2)}$ for all Q^2. Such an ansatz has so far often been used in model calculations. At the reference Q_o^2 of 5 GeV^2, the parametrization selected was

$$x\,G(x) = a\,(1-x)^p\,(1 + c\,x)$$

with $a = 2.63$, $p = 5.9$, $c = 3.5$. Though there is some arbitrariness in choosing this form, it was found that the width of the gluon distribution is well determined by the fit and is only weakly correlated to Λ. This is a consequence of the fact that there are no antiquarks for $x \gtrsim 0.45$. Also other systematic uncertainties, e.g. different assumptions about the shape and size of the strange and charmed sea, influence only weakly the shape of the gluon distribution.

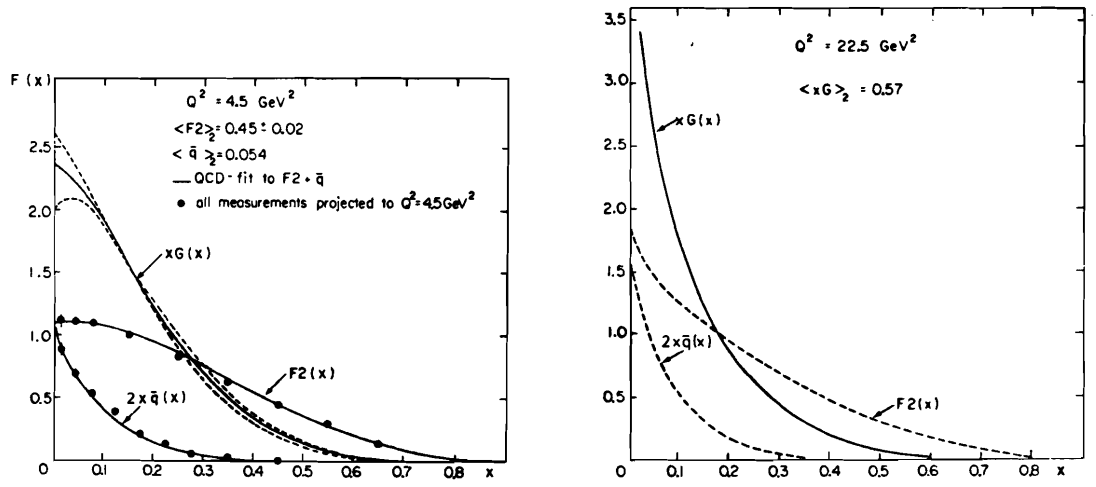

Fig. 11 Shape of $2x\bar{q}(x)$, $F_2(x)$, and $x\,G(x)$ at $Q^2 = 4.5$ and $22.5\ GeV^2$ as evaluated from a leading order QCD fit to $x\bar{q}$ and F_2.

The Charmed Piece of F_2.

The production of heavy quarks proceeds via different mechanisms in electromagnetic respectively neutrino interactions. For the electromagnetic case, the QCD process of photon gluon fusion, i.e. $\gamma g \to c\bar{c}$ can be shown to be the most important source of heavy quark production[36)37)] in the kinematical region explored by present experiments. Once the gluon distribution is known, the cross section can be completely calculated for this process. The model has been tested by the EMC[38)] and the Berkeley-Fermilab-Princeton collaboration[39)] by studying muon induced di- and trimuon final states where the additional muons originate from the semileptonic decay of one or both charmed hadrons. The present data are accurate enough to confirm essential predictions of the model concerning e.g. the relation between dimuon and trimuon production. However, so far it was not possible to extract information on the gluon distribution.

Since little is known about the fragmentation of charmed quarks into the various charmed hadrons and about their subsequent semileptonic decay, additional assumptions are needed for this comparison. For the curves in Fig. 12 it was assumed $D \to \mu\ \nu\ k$ with 10% branching ratio and further a flat c quark fragmentation function $D_c^D(z) = \text{const}$. The figure shows preliminary measurements of the charmed cross section performed by the EMC presented as F_2^{Charm} after multiplication with the appropriate kinematical factors and plotted versus Q^2 for various fixed x. The agreement with predictions from the photon gluon fusion model is acceptable. The data furthermore agree with results from the BFP group. Also shown is the total $F_2^{\mu P}$ for small x. Though the contribution of F_2^{Charm} to $F_2^{\mu P}$ is at most a few percent, there is a sizable contribution to the measured scaling violation of $F_2^{\mu P}$, e.g. at $x = 0.042$ about 30% of the logarithmic slope $\partial F_2/\partial \ln Q^2$ is due to the rise of charm production.

About a year ago Brodsky et al.[40)] have speculated that besides "extrinsic" charm production as described by the photon gluon fusion model, the nucleon contains a long-lived "intrinsic" charm component, i.e. with a probability of about 1% the nucleon finds itself in a $|u\ u\ d\ c\ \bar{c}>$ configuration. The intrinsic c quarks must carry a large fraction of the nucleon momentum, their x distribution is predicted to be

$$c(x) = \bar{c}(x) = 18\,x^2\left[\frac{1}{3}(1-x)(1+10\,x+x^2) - 2\,x\,(1+x)\ln\frac{1}{x}\right].$$

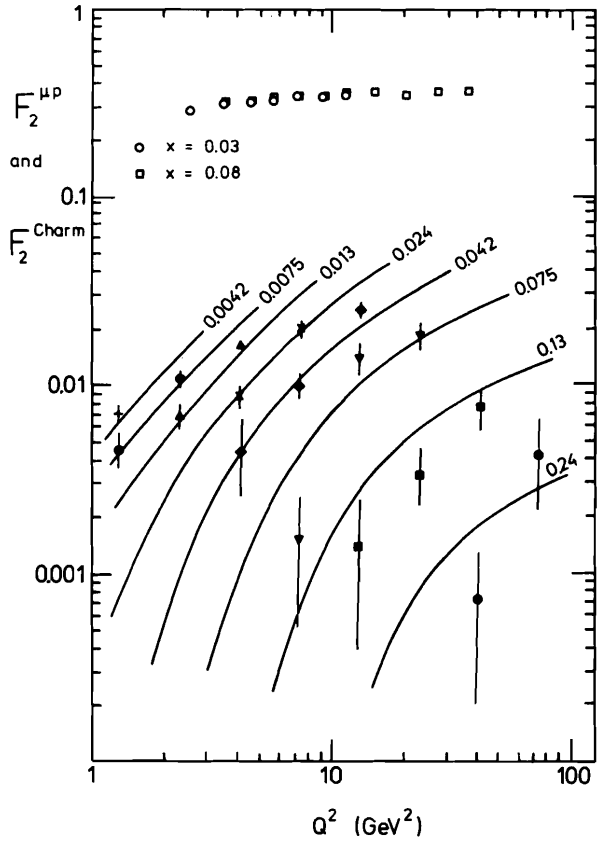

Fig. 12 Charmed piece of F_2 obtained from muon induced like sign plus unlike sign dimuon events plotted versus Q^2 for several fixed x from 0.0042 to 0.24. The curves indicate typical predictions of the photon gluon fusion model. Also plotted is $F_2^{\mu P}$ for x = 0.03 and x = 0.08.

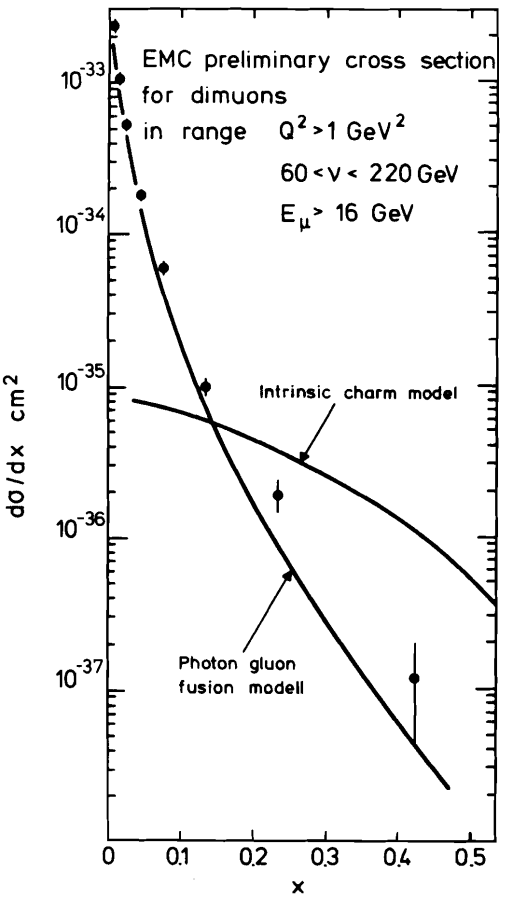

Fig. 13 Differential cross section $d\sigma/dx$ for the sum of the processes $\mu^+N \to \mu^+\mu^-X + \mu^+\mu^+X$ in the range $Q^2 > 1$ GeV^2, $60 < \nu < 220$ GeV and energy of the decay muon $E_\mu > 16$ GeV plotted versus x. The curves show a prediction of the photon gluon fusion model and the expectation for 1% intrinsic charm.

This model is able to explain the diffractive production of charmed hadrons at large longitudinal momentum observed in high energy hadron-hadron collisions. It can be tested by studying dimuon production at large x. Fig. 13 shows preliminary results of the EMC[41]. Plotted is the differential cross section for dimuon production in a defined kinematical range together with predictions from the photon gluon fusion model and the intrinsic charm model.

Notice that the data extend to x = 0.42. Clearly the data fall below the intrinsic charm prediction. This does not rule out intrinsic charm but rather limits the probability for an intrinsic c quark configuration to about 0.3% in the range covered by the data.

4. LEADING AND NEXT-TO-LEADING ORDER QCD FITS

Nucleon structure functions have been quantitatively confronted with QCD predictions since 1977. Here, I will try to answer the question: What have we learned since then, and what is the present situation?

First let us recall that deep inelastic scattering is still a good testing ground for perturbative QCD[42]. From the experimental side we have precise data on structure functions extending up to $Q^2 \sim 250\ GeV^2$. All experiments observe the characteristic scaling violations as expected. From the theoretical side, well known methods exist for the extraction of the mass scale parameter Λ in leading order (LO) and next-to-leading order (NLO).

If the $\overline{MS}$ renormalization scheme[43] is used, all experimental groups find for the numerical values

$$\Lambda_{\overline{MS}} \simeq \Lambda_{LO}$$

$\Lambda_{\overline{MS}}$ is connected to the running coupling constant

$$\alpha_s^{\overline{MS}}(Q^2) = \frac{4\pi}{\beta_o \ln Q^2/\Lambda^2_{\overline{MS}}} \left(1 - \frac{\beta_1}{\beta_o^2} \frac{\ln \ln Q^2/\Lambda^2_{\overline{MS}}}{\ln Q^2/\Lambda^2_{\overline{MS}}}\right)$$

with

$$\beta_o = 11 - \frac{2}{3} N_f , \qquad \beta_1 = 102 - \frac{38}{3} N_f .$$

With the present values of $\Lambda_{\overline{MS}}$ the next-to-leading order term in the brackets of the above equation is approximately 0.18 at $Q^2 = 100\ GeV^2$, and thus indeed a small correction.

For the QCD analysis of the data two theoretically equivalent methods have been employed.

1. Earlier analyses were based on the evaluation of the moment integrals, e.g. of

$$M_n(Q^2) = \int_o^1 dx\, x^{n-2}\, F_2(x,Q^2), \text{ etc.}$$

The advantages of this procedure are mainly:

- Clear theoretical predictions.
- It is straightforward to include second order corrections even for structure functions containing singlet contributions (like F_2).

However, there are serious disadvantages:

- The disadvantage weighting heaviest in the eyes of an experimentalist is the fact that one cannot use the high Q^2 data since they are measured only at a few x values.
- Also strong correlations exist between various orders n since the same data are used several times. This fact has to be taken into account for the fits. If correlations are ignored, Λ and its error come out differently.
- At lower Q^2 the moments contain severe contributions originating from the elastic peak and the resonance region.

Still the moment method is useful, e.g. for the evaluation of the ratios of the anomalous dimensions. A recent analysis of the log M_5 versus log M_3 dependence of the Nachtmann moments[44] evaluated from the CDHS data[34] results in $d_5/d_3 = 1.68 \pm 0.11$. The QCD values are 1.46 in LO and 1.57 in NLO, while for scalar gluons a ratio of 1.12 is expected.

2. The procedure mainly applied by the experimental groups directly uses the full x,Q^2 dependence of the structure functions by numerically solving the Altarelli-Parisi equations. Such solutions can be of the form

$$F(x,Q^2) = \int_x^1 dy\ b(x,y;\ Q^2,Q_o^2)\ \ F(y,Q_o^2),$$

where the kernel b can be expanded in a power series in α_s and is known from perturbation theory up to order α_s^2.

The advantages of the direct method are:

- All measured data points can fully be incorporated.
- One can easily study the influence of cuts, e.g. in $W^2 \simeq Q^2(1-x)/x$ on the outcome of the fit.
- One can rely on three well documented numerical procedures originating from Gonzàles-Arroyo, López and Yndurain[45] LO, NLO
  Abbott and Barnett[35] LO, NLO
  Bialas and Buras[46] NLO .

  A slight disadvantage is due to the necessity of selecting an explicit input parametrization of the x dependence at some reference Q_o^2, usually

$$F^{NS}(x,Q_o^2) = C\ x^{\alpha}\ (1-x)^{\beta}\ \ (1 + \gamma x).$$

  The constant C might be fixed by the Gross- Llewellyn Smith sum rule[47].

In a contribution to this conference a new method for an approximated solution of the QCD evolution equations has been proposed by Isaev et al.[48]. So far this method has been applied to earlier data sets.

There exists a well defined prescription for including (a part of) target mass effects[44)49] by using the Georgi-Politzer[50] variable

$$\xi = 2x / (1 + \sqrt{1 + 4M^2 x^2/Q^2})$$

instead of x. In the non-singlet case the function $F(\xi,Q^2)$, which then has to be inserted in the Altarelli-Parisi equations, is connected to the measured function $F^{NS}(x,Q^2)$ by[50)35]

$$F^{NS}(x,Q^2) = \frac{x^2}{\xi^2\ (1 + 4M^2 x^2/Q^2)}\ \ F(\xi,Q^2) + \frac{4M^2 x^3}{Q^2\ (1 + 4M^2 x^2/Q^2)^{3/2}} \int_{\xi}^{1} \frac{dy}{y^2}\ \ F(y,Q^2) .$$

Target mass effects contribute, like other higher twist effects, terms proportional to powers of $1/Q^2$ to the structure function[51]. Generally one may write[10]

$$F_i(x,Q^2) = F_i^{QCD}(x,Q^2)\left(1 + \frac{h_4(x)}{Q^2} + \frac{h_6(x)}{Q^4} + \ldots\right),$$

where h_4, h_6 are unknown functions of x originating from incalculable hadronic matrix elements of twist 4, twist 6 operators. Examples of higher twist contributions are diquark scattering, quark mass effects, primordial $p_\perp$ effects, resonance contributions, etc. Principally even the sign of the functions h_4, h_6 is unknown. One knows, however, that the influence of higher twist effects increases with x, functional forms which have been used in the literature[10)2)] are $h_4(x) \propto 1/(1-x)$ or $h_4(x) \propto x/(1-x)$.

It has been argued that the inclusion of the target mass formalism tends to overcorrect the $1/Q^2$ effects[52]. Anyway, it turns out that the data are accurate enough to perform fits with $h_4(x)$ essentially free to adjust itself at each x value. I will return to this aspect later.

Let me first discuss the new results on QCD fits presented this year by six collaborations. There are some differences in the details of the analysis, and it is therefore interesting to compare the work of the different groups.

ABBSL (Gargamelle)[18]

The group evaluated xF_3 and $F_2^{\nu N}$ from a data sample of 3000 neutrino and 3800 antineutrino events measured with the CERN wide band beam. The muon is detected with the external muon identifier. In this work the Q^2 region $0.5 < Q^2 < 50$ GeV^2 is covered with a single experiment. In the analysis of the structure functions, Fermi motion corrections have been applied. Radiative corrections are estimated to be small and are ignored. A value of $R = 0.1$ is assumed.

The comparison with QCD predictions is performed with a non-singlet structure function defined as xF_3 for $x < 0.4$ and F_2 for $x > 0.4$. Fits in LO and NLO using the methods of Bialas and Buras and of Gonzàles-Arroyo et al. with the boundary condition $F^{NS}(x,Q_o^2) = C\, x^\alpha (1-x)^\beta$ result in the values of Λ given in Table 3.

Table 3 Results of QCD fits of the GGM collaboration

Q^2 range (GeV^2)	Fit	Λ_{LO} or $\Lambda_{\overline{MS}}$ (MeV)
> 2	LO	$190\ ^{+\ 160}_{-\ 120}$
> 2	NLO	$150\ ^{+\ 150}_{-\ 110}$
> 0.5	LO with target mass corr.	$0\ ^{+\ 20}_{-\ 0}$
> 2	LO with target mass corr.	$20\ ^{+\ 90}_{-\ 20}$

Taking into account a twist 4 contribution with $h_4(x) = \mu^2 x/(1-x)$ yields for a LO fit in the region $Q^2 > 2$ GeV^2 $\Lambda < 700$ MeV with 90% confidence level and $-0.8 < \mu^2 < 0.7$ GeV^2. Fig. 14 shows the data together with several fits. The fact that the inclusion of target mass effects leads to $\Lambda \simeq 0$ (ξ scaling) might indicate an overcorrection at low Q^2.

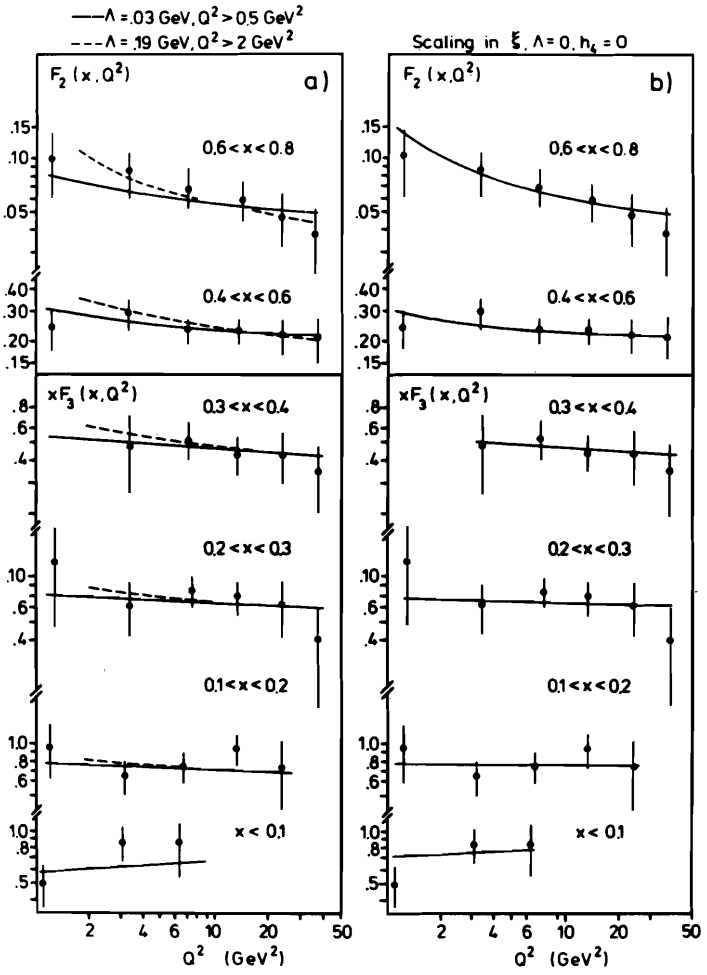

Fig. 14

Non-Singlet structure function obtained from GGM plotted versus Q^2 for various x intervals. The errors contain 10% systematic uncertainty added linearly to the statistical error. The uncertainty due to neutrino flux normalization is not included. The curves indicate

a) LO predictions fitted with Λ = 30 respectively 190 MeV;

b) fit with scaling in ξ with Λ = 0.

ABCDLOS (BEBC)[14]

xF_3 and $F_2^{\nu N}$ are determined from 3100 neutrino and 1100 antineutrino events, taken with the CERN narrow band beam using additional low Q^2 data from Gargamelle SPS runs. Radiative corrections have been applied to the data. For the determination of F_2 the validity of the Callan-Gross relation $2\,xF_1 = F_2$ is assumed. The data cover the range $0.02 \leq Q^2 \leq 70$ GeV^2 for $.0 < x < 0.1$ and $0.4 \leq Q^2 \leq 70$ GeV^2 for $0.6 < x < 1$. At large x both structure functions show the characteristic decrease with increasing Q^2. At small x values F_2 increases with Q^2, xF_3 shows no obvious Q^2 dependence for $Q^2 > 1$ GeV^2. Within errors there is good agreement with the results of other neutrino experiments.

A comparison with QCD predictions is made by evaluating the Nachtmann moments. The n = 1 moment of xF_3 has to satisfy the Gross-Llewellyn Smith sum rule which reads, after inclusion of next-to-leading order corrections,

$$\int_0^1 dx\, F_3(x,Q^2) = 3\left[1 - \frac{12}{(33 - 2N_f)\,\ln Q^2/\Lambda^2}\right].$$

The data show agreement with a value of 3 for $Q^2 > 1$ GeV^2 and thus prefer a small value of $\Lambda < 100$ MeV.

A fit to the x,Q^2 dependence of xF_3 for $0.02 < x < 0.4$ and to F_2 for $x > 0.4$ using the method of Gonzàles-Arroyo et al. and including target mass corrections yields the values of Table 4.

Table 4 QCD fits of the ABCDLOS collaboration.

Q^2 range (GeV^2)	Fit	Λ_{LO} or $\Lambda_{\overline{MS}}$ (MeV)
> 2	LO	210 ± 95
> 2	NLO	$145 \begin{smallmatrix} + 95 \\ - 35 \end{smallmatrix}$

Both Λ values are in good agreement with the results obtained from fits to the Nachtmann moments. The group also reports on indications of higher twist effects.

CHARM[20]

The group presents xF_3 and $F_2^{\nu N}$ data obtained from 6500 neutrino and 4500 antineutrino events measured with a fine grain target calorimeter in the narrow band beam. In the analysis the validity of the Callan-Gross relation is assumed, Fermi motion effects and radiative corrections are included.

For the comparison with QCD a fit is performed to xF_3 and to F_2 using the LO method of Buras and Gaemers[53] with the ansatz

$$x\, q_{\substack{sea \\ glue}}(x,Q^2) = A(Q^2)\ (1-x)^{\eta_s(Q^2)}$$

setting $\eta_{glue} = \eta_{sea}$ (which is only a very rough approximation). With the cuts $Q^2 > 3$ GeV^2 and $x < 0.65$ one finds

$$\Lambda_{LO} = 290 \pm 120 \pm 100 \text{ MeV} .$$

The second error is due to systematical uncertainties.

The group also studied the effect on Λ due to various changes of the assumptions made in the analysis, some results are given in Table 5.

Table 5 Sensitivity of Λ to modifications of the analysis.

Change in Analysis	Variation of Λ_{LO} (MeV)
No Fermi correction	- 106
No Fermi and no radiative correction	- 167
R = 0.1 (instead $2\,xF_1 = F_2$)	- 82
$\eta_{glue} = \eta_{sea} - 1$	+ 25

A fit including higher twist contributions with

$$F_2 = F_2^{QCD} \left(1 + \frac{\mu_1^2}{Q^2 (1 - x)} + \frac{\mu_2^4}{Q^4 (1 - x)^2}\right)$$

results in $\Lambda = 240 \pm 120$ MeV, $\mu_1 = 0.28 \pm 0.24$ GeV, $\mu_2 = 0.11 \pm 2.5$ GeV.

CDHS[1)2)34)]

The CDHS collaboration accumulated by far the highest statistics of all neutrino experiments. xF_3, $F_2^{\nu N}$ and $x\bar{q}$ are determined from 94 000 neutrino and 26 000 antineutrino events measured with the narrow band beam. For the extraction of $x\bar{q}$ also 150 000 antineutrino events measured with the wide band beam are included. The data analysis contains radiative corrections but no Fermi motion corrections.

1. Fits to the non-singlet structure function.

The fits are performed to a combined data set of non-singlet structure functions defined as xF_3 and in addition as

$$2\, xF_1 / \sqrt{1 + Q^2/\nu^2} = F_2 \sqrt{1 + Q^2/\nu^2}/(1 + R)$$

for $x > 0.4$ assuming $R = 0.1$. The Q^2 range is further extended by including for $x > 0.4$ also the function $F_+ = 1/2\,(2\, xF_1^{\nu N} + xF_3^{\nu N})$ derived from 300 GeV neutrino data measured at large y. Included in the fit are target mass corrections and also a correction for the W propagator term with $M_W = 80$ GeV. The Abbott-Barnett program is used with the boundary condition

$$\xi\, F_3\,(\xi, Q_o^2) = \alpha\, \xi^{\beta}\, (1 - \xi)^{\gamma}\, (1 + \delta\xi)\ .$$

Pure QCD fits with the cut $W^2 > 11$ GeV^2 result in:

Table 6 Fits of the CDHS collaboration

Q^2 (GeV^2)	Fit	Λ_{LO} or $\Lambda_{\overline{MS}}$ (MeV)	χ^2/DF
> 2	LO	190 ± 80	156/107
> 2	NLO	210 ± 80	155/107
> 10	LO	140 ± 60	80/72

Again second order corrections are found to be small when working in the $\overline{MS}$ scheme. Taking into account some systematical errors, $90 < \Lambda_{\overline{MS}} < 320$ MeV with 90% confidence level.

To test for the presence of higher twist terms, all data with $Q^2 > 2$ GeV^2 and also some SLAC ed data with $x \geq 0.5$ are included in order to increase the sensitivity. No acceptable fit is found if only a twist 4 term of the form $h_4(x) = \mu^2\, x/(1-x)$ is taken into account, and Λ is set to be 0. An acceptable fit is obtained with $\Lambda_{LO} = 200$ MeV and $\mu^2 = 0.84 \pm 0.10$ GeV^2 (χ^2/DF = 184/145). The data together with this fit are displayed in Fig. 15.

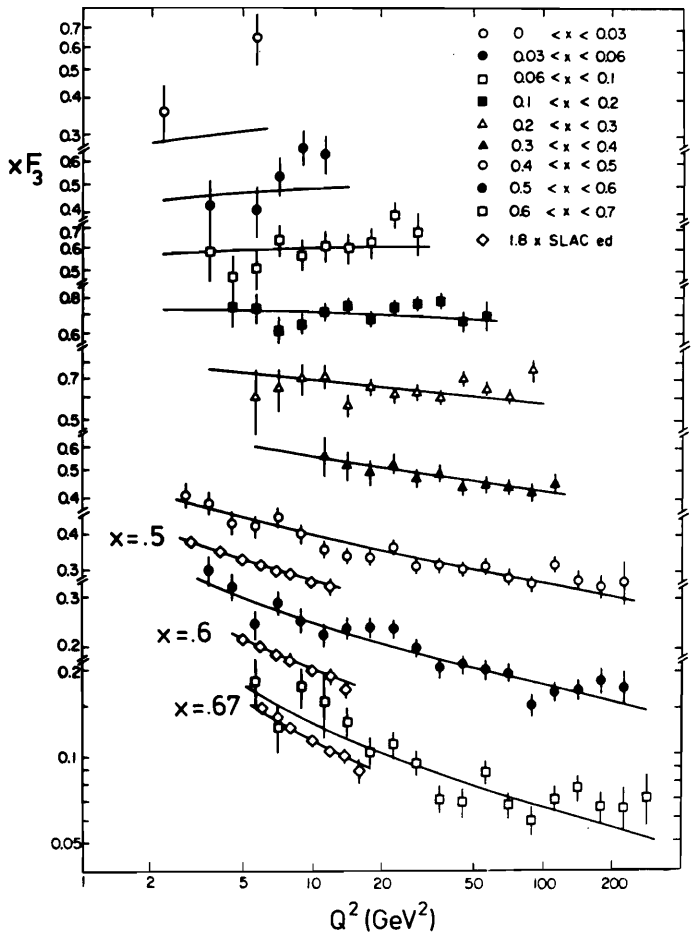

Fig. 15

Non-singlet structure function xF_3 from CDHS plotted versus Q^2 for various x. Also shown are SLAC ed data for $x \geq 0.5$. The curves represent a leading order QCD fit including a twist 4 term.

Second order fits with different parametrizations of the twist 4 function $h_4(x)$ yield:

Table 7 NLO order fits from CDHS including twist 4 contributions

$h_4(x)$	$\Lambda_{\overline{MS}}$ (MeV)	μ^2 (GeV^2)	χ^2/DF
$\mu^2 \frac{x}{1-x}$	240^{+70}_{-80}	$.74^{+.38}_{-.31}$	177/145
$\mu^2 \frac{1}{1-x}$	430 ± 40	-.15 ± .10	178/145

In both cases $\Lambda_{\overline{MS}}$ and μ^2 are strongly correlated. The result depends critically on the ansatz used for $h_4(x)$. Since there is no theoretical guideline with respect to the functional form of $h_4(x)$, it is of the utmost importance that one tries to measure this function.

2. Combined Analysis of F_2 and $x\bar{q}$.

These are the data with the highest statistical accuracy. On the other hand, the QCD analysis of the x,Q^2 dependence of singlet structure functions can so far be performed only in leading order. Restricting the F_2 and $x\bar{q}$ data to the region $W^2 > 20$ GeV^2 in order to suppress possible higher twist contributions one finds $\Lambda_{LO} = 200 \pm 20$ MeV.

EMC[23]

Fully analyzed data from hydrogen and iron targets are presented. The $F_2^{\mu p}$ values are based on about 100 000 events measured at 120 GeV beam energy and 140 000 events measured at 280 GeV, the $F_2^{\mu N}$ data base on 540 000 events measured at 120 GeV, 200 000 events measured at 250 GeV, and 70 000 events measured at 280 GeV.

Radiative corrections include the exact calculation of hard bremsstrahlung from the muon in lowest order of α and a calculation of other electromagnetic contributions in all orders of α. The energy distribution of single hard photons originating from internal bremsstrahlung has been measured and was found to be in good agreement with the calculations[54].

For the extraction of the F_2 data a value of $R = 0$ was used. Effects due to the Fermi motion and the binding of the nucleons inside the iron nucleus have been calculated and found to be a few percent in the x range ($x \leq 0.65$), where $F_2^{\mu N}$ values are presented. Therefore no Fermi motion corrections are applied. The hydrogen data are clearly free of such effects. It is therefore interesting to compare the results of QCD fits obtained for the two targets.

Leading and next-to-leading order fits have been performed using the techniques of Abbott and Barnett and of Gonzàles-Arroyo et al. Target mass corrections are not included.

In a first step it was assumed that the F_2 data at large x can be compared with QCD predictions for a pure non-singlet structure function with boundary condition $F_2(x,Q_o^2) = c\, x^\alpha\, (1-x)^\beta\, (1+\gamma\, x)$ at $Q_o^2 = 4$ GeV^2. It has been checked that this procedure leads to reliable results in the region $x \geq 0.25$ by substracting from the measured values of F_2 the contribution due to sea quarks, evaluated either from the parametrization of Glück et al.[30] or by calculating the Q^2 evolution of the sea starting from the CDHS parametrization of the gluon distribution. The results of some representative fits are:

Table 8 Fits to the EMC H_2 and Fe data

Data	Fit	Λ_{LO} or $\Lambda_{\overline{MS}}$ (MeV)
Fe $Q^2 \geq 4.5$ GeV^2	LO	$122\ ^{+\ 12\ +\ 86}_{-\ 11\ -\ 32}$
	NLO	$170\ ^{+\ 155}_{-\ 105}$
H_2 $Q^2 \geq 7$ GeV^2	LO	$110\ ^{+\ 143}_{+\ \ 74}$
	NLO	$145\ ^{+\ 150}_{-\ \ 90}$

The Λ values obtained from the data of both targets agree well, the changes of the numerical value by going from leading order to next-to-leading order in the $\overline{MS}$ scheme are small.

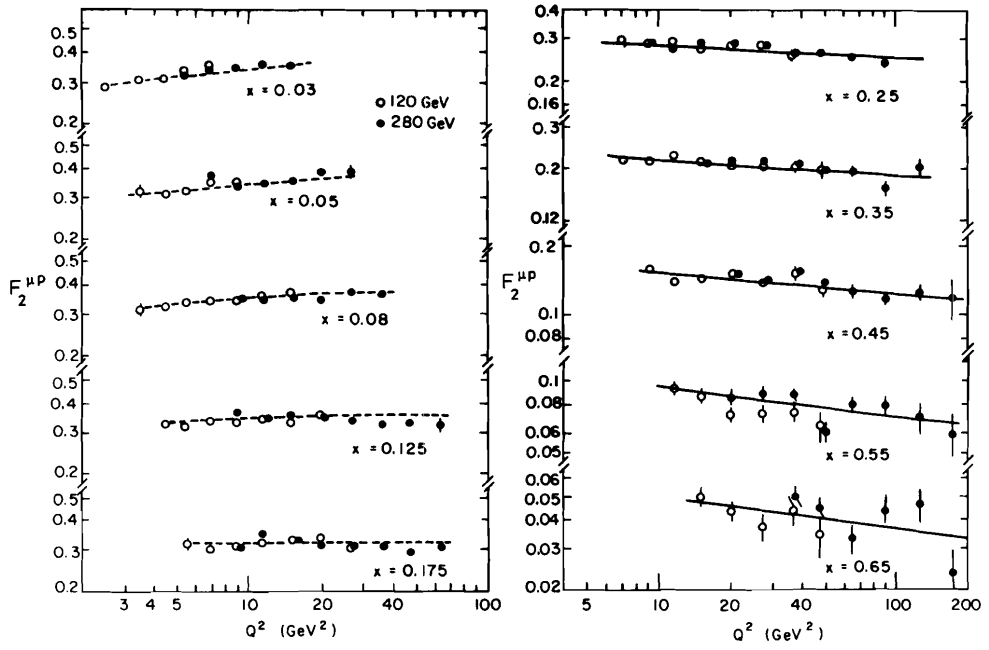

Fig. 16 $F_2^{\mu p}$ from EMC with statistical errors compared to leading order QCD fits as described in the text.

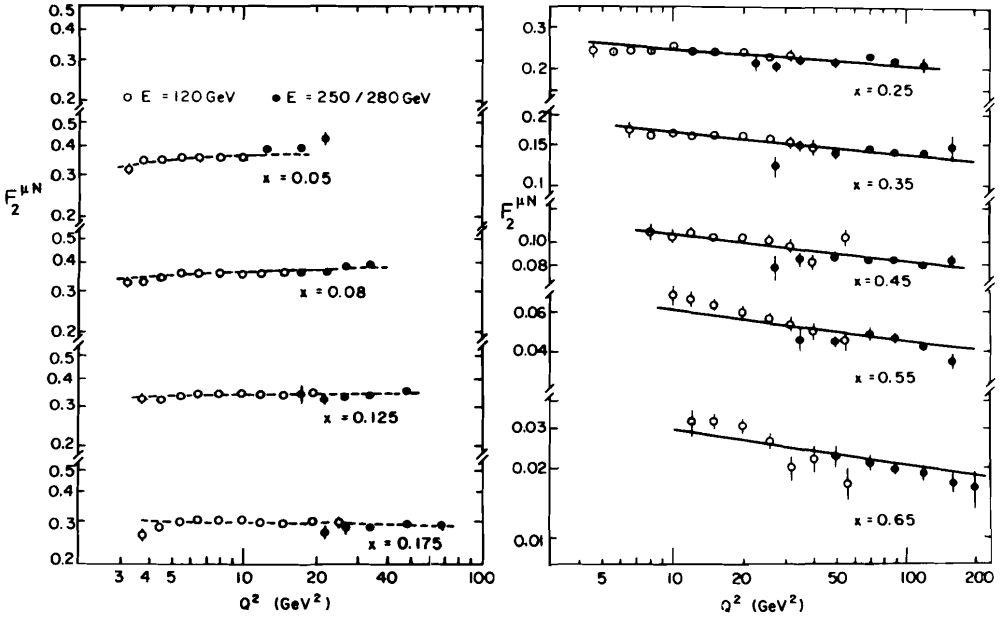

Fig. 17 $F_2^{\mu N}$ obtained from measurements with an iron target compared to different leading order QCD fits.

In a second step the Λ_{LO} values of Table 8 were used to extend the QCD prediction to the region of small x where sea quark contributions are important. With Λ fixed a fit is made to all data using the singlet evolution equations. To reduce the influence of charm threshold, at $x = 0.03$ and 0.05 only the point with the lowest Q^2 was included in the fitting procedure. The results for the hydrogen data are shown in Fig. 16. The solid curves indicate the non-singlet fit for $x \geq 0.25$, the broken curves the singlet fit. A similar procedure has been applied to the iron data (Fig. 17).

BCDMS[24)25)]

The group published fully analyzed $F_2^{\mu N}$ data based on 100 000 events taken at a beam energy of 120 GeV and the same number of events taken at a beam energy of 200 GeV, both with a carbon target. Preliminary data from 200 000 events measured at 280 GeV are also presented.

The analysis includes radiative corrections but no correction for Fermi motion effects. For the extraction of F_2 a value of $R = 0$ is assumed.

For QCD fits in leading and next-to-leading order the method of Gonzàles-Arroyo et al. is applied. Since the data extend over the region $.3 < x < .7$, it seems justified to consider F_2 as a non-singlet structure function with the boundary condition $F_2(x,Q_o^2) \propto x^{\alpha} (1-x)^{\beta}$. Furthermore, since $Q^2 > 25$ GeV^2 higher twist effects can be expected to be small. Resulting values of Λ are summarized in Table 9.

Table 9 Fits of the BCDMS collaboration

Data	Fit	Λ_{LO} or $\Lambda_{\overline{MS}}$ (MeV)
120, 200 GeV carbon	LO	$85 \begin{smallmatrix} + 60 + 90 \\ - 40 - 70 \end{smallmatrix}$
	NLO	$85 \begin{smallmatrix} + 53 + 80 \\ - 40 - 67 \end{smallmatrix}$
120, 200 GeV plus 280 GeV (prelim.) carbon	LO	$10 \begin{smallmatrix} + 10 + 36 \\ - 6 - 10 \end{smallmatrix}$

Again the first error indicates the statistical and the second error the systematical uncertainty. Because of the small logarithmic slope of F_2, the above values of Λ are very sensitive with respect to a small change in the relative normalization between the data taken at different energies, e.g. an increase of 2% of the 120 GeV data changes the first value of Λ in Table 9 by + 70 MeV and the last value by a factor of 2.5. The value of Λ obtained from the fit including preliminary 280 GeV data must therefore be considered with great caution.

Fig. 18 shows the data together with the LO fit to the 120 and 200 GeV points (solid line) and the LO fit including the preliminary 280 GeV data (broken line).

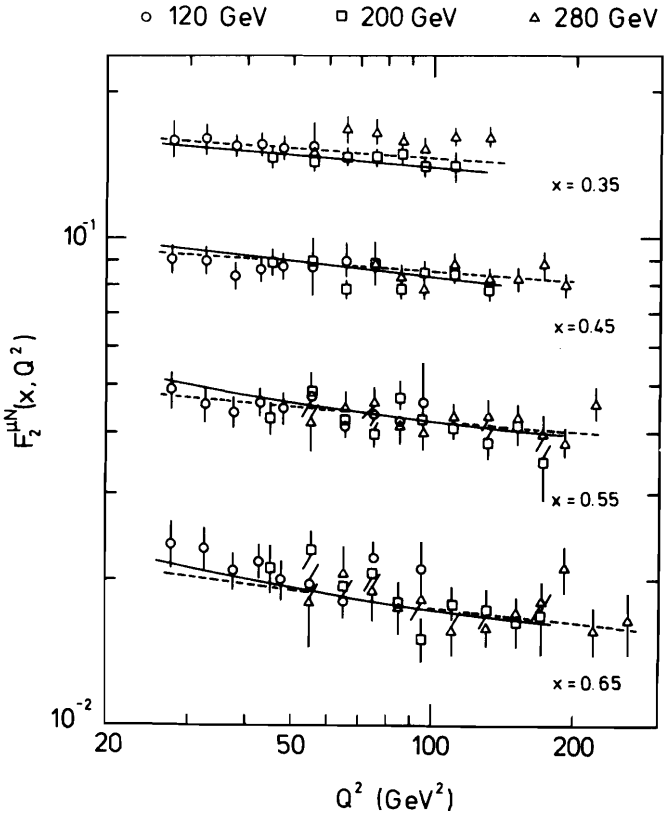

Fig. 18

$F_2^{\mu N}$ from BCDMS. The errors are a quadratic superposition of statistical and systematical uncertainties. The curves indicate leading order QCD fits with Λ = 85 MeV (solid line) and Λ = 10 MeV (broken line).

Λ_{LO} (GeV)	CHIO + SLAC	BEBC + GGM	CDHS + SLAC	CHIO + SLAC	MSU-F + SLAC	EMC	CDHS	BCDMS	GGM	CHARM	BEBC + GGM
	$F_2^{\mu p,\mu d}$	xF_3	xF_3 . F_2	$F_2^{\mu p,\mu d}$	F_2	$F_2^{\mu p,\mu Fe}$ $x \geq .25$	xF_3 F_2 for $x > .4$	F_2 x .3	xF_3 F_2 for $x > .4$	F_2 xF_3	xF_3
.8											
.6											
.4											
.2											
.1											
0											
Q^2	3-50	1-60	6-75	3-40	3-120	3-200	2-280	25-280	2-50	3-180	2-70
	N. Moments		B.G.	Mom.	A.P. Evolution Equations						
	1977	1978	1979		1980	1981					

Fig. 19 Development of Λ_{LO} values. The first five entries are from References[55)56)57)11)58)].

What can we conclude from all this work? The development of Λ values as obtained from leading order QCD fits by the various groups is shown in Fig. 19. With increasing range of Q^2 covered by the experiments, there is a clear trend towards smaller values of Λ, a direct consequence of the fact that scaling violations observed at high Q^2 are small.

The scaling violations measured in all recent experiments can be parametrized by $50 < \Lambda_{LO} < 250$ MeV. The inclusion of next-to-leading order corrections changes the results obtained from the leading order fits only slightly when working in the $\overline{MS}$ scheme.

Translating into α_s, one finds for the high statistics experiments covering the Q^2 range above 100 GeV^2:

Table 10 $\Lambda_{\overline{MS}}$ and $\alpha_s^{\overline{MS}}/\pi$ from recent experiments

Group	$\Lambda_{\overline{MS}}$ (MeV)	$\alpha_s^{\overline{MS}}/\pi$ at $Q^2 = 100$ GeV^2
CDHS, Fe	$210 \begin{smallmatrix}+\ 80\\-\ 70\end{smallmatrix}$	0.050 ± 0.004
EMC, H_2	$145 \begin{smallmatrix}+\ 150\\-\ 90\end{smallmatrix}$	0.046 ± 0.008
Fe	$170 \begin{smallmatrix}+\ 155\\-\ 105\end{smallmatrix}$	0.048 ± 0.008
BCDMS, C	$85 \begin{smallmatrix}+\ 96\\-\ 78\end{smallmatrix}$	$0.041 \begin{smallmatrix}+\ 0.007\\-\ 0.013\end{smallmatrix}$

If one takes the liberty to consider these as independent measurements of $\Lambda_{\overline{MS}}$, one finds the average values

$$\Lambda_{\overline{MS}} \simeq 160 \begin{smallmatrix}+\ 100\\-\ 80\end{smallmatrix}, \quad \frac{\alpha_s^{\overline{MS}}}{\pi} \simeq 0.047 \pm 0.006$$

at $Q^2 = 100$ GeV^2 (increasing the errors to 2 σ).

Separation of Higher Twist Contributions from the Leading Twist 2 Effects.

One can try to go one step further and separate the $1/Q^2$ or $1/Q^4$ power behaviour due to higher twist effects from the leading twist 2 contribution. The basis for these studies is the enormous range in Q^2 covered nowadays by high precision data.

Let me first summarize results obtained by Eisele[34] of the CDHS group who used SLAC ed data in addition to CDHS F_2 and xq data. He finds:

1. From a pure QCD fit to the CDHS data with a cut at $W^2 > 20$ GeV^2 in order to reduce higher twist effects, $\Lambda_{LO} = 200 \pm 20$ MeV.
2. Extrapolating this fit in the kinematical region covered by SLAC data (typically $Q^2 \sim 8$ GeV^2), one observes that higher twist corrections have to be included at large x. This conclusion remains unchanged if target mass corrections are calculated.

3. It is not possible to increase the value of Λ significantly (e.g. to 400 MeV). The reason is that one would need a very broad gluon distribution in order to understand the data. However, this is excluded due to the fact that $x\bar{q}$ vanishes for $x \gtrsim 0.45$. Thus Λ cannot be larger than about 250 MeV.

One can then fit the expression

$$F_2(x,Q^2) = F_2^{QCD}(x,Q^2) + F_2^{HT}(x,Q^2),$$

where $$F_2^{HT}(x,Q^2) = h_4(x)/Q^2 \quad \text{or} \quad h_6(x)/Q^4$$

to all available data at each of the various fixed x values. The resulting values of the higher twist part of F_2 are plotted in Fig. 20 as a function of x for $Q^2 = 8$ GeV^2. In the fits Λ was fixed to 200 MeV, target mass effects were included.

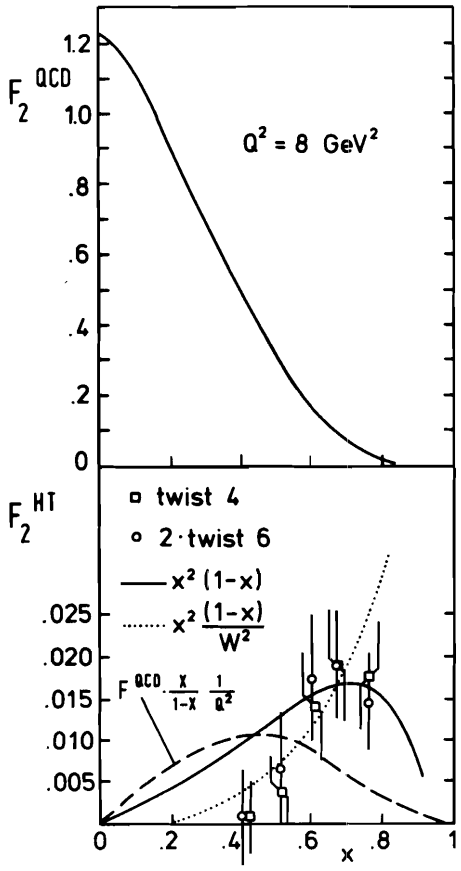

Fig. 20

QCD and higher twist contributions of $F_2^{\nu N}$ at $Q^2 = 8$ GeV^2 obtained from fits to the CDHS and SLAC ed data. Target mass corrections are already included in F_2^{QCD}. The solid curve in the lower part represents the diquark model prediction of Donnachie and Landshoff.

The higher twist contribution of F_2 is positive for $x > 0.5$, its shape agrees reasonably well with the predictions of a diquark model[31] but is incompatible with the functional form $F_2^{HT} \propto F_2^{QCD}\, x/(1-x)/Q^2$ which was previously favoured.

In a somewhat related way the x dependence of the twist 4 contribution of F_2 was studied by M. Leenen[59] of the EMC by combining SLAC ep data and EMC μp data for $x \geq 0.25$. For the SLAC data an average value of $R = \sigma_L/\sigma_T$ of 0.21 was used, for the EMC data $R = 0$ was assumed. The relative normalization between SLAC and EMC data can then be fixed by a single factor obtained from a comparison of the data in the region of the kinematical overlap, EMC/SLAC = 0.90.

This analysis is not affected by uncertainties originating from Fermi motion effects and can therefore be extended to large x. Due to the large number of data points it was possible to fit simultaneously both the leading twist 2 contribution as well as the twist 4 correction using the expression

$$F_2(x,Q^2) = F_2^{QCD}(x,Q^2)\ (1 + h_4(x)/Q^2).$$

Here, F_2^{QCD} is considered as non-singlet structure function parametrized in next-to-leading order in the $\overline{MS}$ scheme. Target mass corrections are not included but rather considered as a part of the twist 4 term. Since the Q^2 variation of F_2 is studied for a finite number of x bins, the function h_4 was allowed to adjust itself for each value of x separately. From the fit a value of $\Lambda_{\overline{MS}} = 130 + 50 - 40$ MeV is obtained. The resulting values of $h_4(x)$ are plotted in Fig. 21.

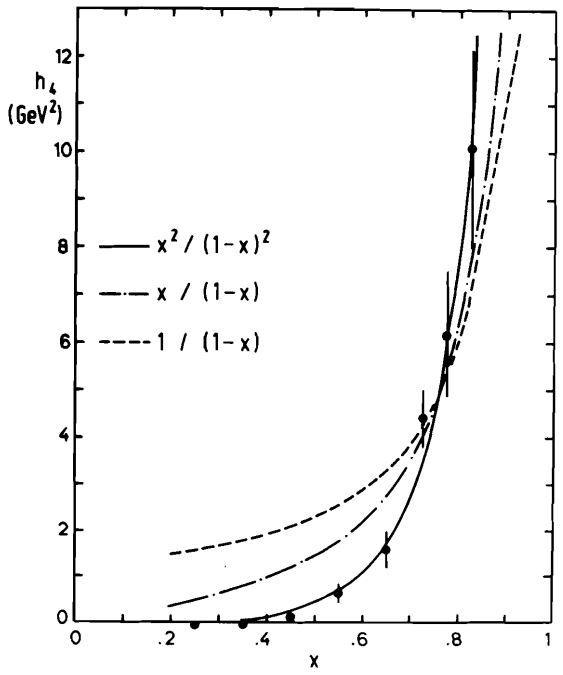

Fig. 21

$h_4(x)$ obtained from NLO fits to the SLAC ep and EMC μp data using the ansatz $F_2 = F_2^{QCD}\ (1+h_4(x)/Q^2)$.

Again h_4 is found to be positive for $x > 0.5$ raising steeply with x. An adequate parametrization is

$$h_4(x) \propto x^2/(1 - x)^2 ,$$

while the usual forms $h_4 \propto x/(1 - x)$ or $1/(1 - x)$ are not in agreement with this evaluation.

It should be mentioned that the results do not significantly change if a value of $R = 0$ is assumed for the SLAC data. Also a subtraction of the sea

contribution of F_2 as evaluated from the CDHS measurements of $x\bar{q}$ does not alter the results.

We can conclude: Both studies show that the higher twist contribution is positive for $x > 0.5$ and the x dependence is steeper than previously assumed.

SUMMARY

1. Precise data on $F_2^{\mu p}$, $F_2^{\mu N}$, $F_2^{\nu N}$, xF_3 extending up to $Q^2 \sim 200$ GeV^2 are now available. Good agreement is observed between all recent experiments except for an unresolved problem which arises in the comparison of the small x values of xF_3, $F_2^{\nu N}$ from CDHS versus the preliminary data from CFRR.

2. The Q^2 evolution of the light antiquark sea is known from the high statistics antineutrino data. With this information at hand it is possible to evaluate also the Q^2 evolution of the gluon distribution function.

3. New measurements of $\mu n/\mu p$ and $\bar{\nu}n/\bar{\nu}p$ or $\nu n/\nu p$ ratios confirm the strong decrease of the ratio of d quarks over u quarks with increasing x. The ratios show no significant variation with Q^2 at fixed x in agreement with the expectation from QCD.

4. The charmed piece of $F_2^{\mu N}$ contributes about 30% to the scaling violation measured at small x. No evidence for a hard intrinsic charm component with a probability larger than 0.3% is found.

5. QCD fits performed by the experimental groups result in small values of the mass scale parameter Λ, typically $50 < \Lambda < 250$ MeV. Averaging the values obtained from the high statistics experiments gives

$$\Lambda_{\overline{MS}} \simeq 160 \begin{smallmatrix} + 110 \\ - 80 \end{smallmatrix} \text{ MeV}, \quad \alpha_s^{\overline{MS}} = 0.148 \pm 0.019 \quad \text{at} \quad Q^2 = 100 \text{ GeV}^2 .$$

6. Due to the high precision and the large Q^2 range of the data sets one can now study higher twist contributions to F_2 separately.

ACKNOWLEDGEMENT

I would like to thank H. Wahl, F. Eisele, U. Amaldi, G. Smadja, P. Fritze, and H. Weerts for providing me with much of the information contained in this review. I also thank many colleagues of the European Muon Collaboration for innumerable discussions and my scientific secretary, Ch. Nietzel, for his help in preparing the written version.

REFERENCES AND FOOTNOTES

1. Wotschack, J., "νN: Determination of Nucleon Structure Functions", Proceedings of this conference.

2. Wahl, H., "Deep Inelastic Lepton-Hadron Scattering: Structure Functions", Proceedings of the Internat. Conference on High Energy Physics, Lisbon (1981).

3. Sciulli, F., Proceedings of the XX International Conference on High Energy Physics, Madison (1980), part 2, 1278.

4. For recent reviews on perturbative QCD in connection with deep inelastic scattering, see e.g. A.J. Buras, Rev. Mod. Phys. 52 (1980) 199; E. Reya, Perturbative Quantum Chromodynamics, Phys. Report 69 (1981) 195.

5. For muon scattering $\sigma_o = 4\pi\ \alpha^2\ ME/Q^4$, for neutrino scattering $\sigma_o = G^2\ ME/\pi$ and $d^2\ \sigma/dx/dy \simeq d^2\ \sigma^{\nu N}/dx/dy + d^2\ \sigma^{\bar{\nu}N}/dx/dy$.

6. CERN-Dortmund-Heidelberg-Saclay Collaboration, H. Abramowicz et al., Report CERN-EP/81-50 (1981).

7. Altarelli, G., and G. Martinelli, Phys. Lett. 76 B (1978) 89.

8. Bodek, A. et al., Phys. Rev. D 20 (1979) 1471.

9. Mestayer, M.D., SLAC Report No. 214 (1978); The SLAC data of Fig. 2 and the QCD plus diquark model prediction are reproduced from Ref. 10.

10. Abbott, L.F., W.B. Atwood, and R.M. Barnett, Phys. Rev. D 22 (1980) 582.

11. Gordon et al., Phys. Rev. D 20 (1979) 2645.

12. European Muon Collaboration (CERN-DESY-Freiburg-Kiel-Lancaster-LAPP-Liverpool-Oxford-Rutherford-Sheffield-Turin-Wuppertal), J.J. Aubert et al., to be published.

13. Benvenuti, A., et al., Phys. Rev. Lett. 42 (1979) 1317.

14. Aachen-Bonn-CERN-Athens-London-Oxford-Saclay Collaboration, H. Deden et al., "Total Cross Sections and Nucleon Structure Functions", contribution to the ν 81 International Conference on Neutrino Physics and Astrophysics, Wailea (1981), presented by P. Fritze.

15. Fermilab-IHEP-ITEP-Michigan Collaboration, V.V. Ammosov et al., "Inclusive Charged-Current Antineutrino-Nucleon Interactions at High Energies", paper No. 11; submitted to this conference.

16. Amsterdam-CERN-Hamburg-Moscow-Rome Collaboration, M. Jonker et al., Phys. Lett. 102 B (1981) 67.

17. Altarelli, G., and G. Parisi, Nucl. Phys. B 126 (1977) 298.

18. Aachen-Bergen-Brussels-CERN-Milan-Orsay-Strasbourg-London Collaboration, J.G. Morfin et al., Phys. Lett. 104 B (1981) 235, and Aachen-Bergen-Brussels-Strasbourg-London Collaboration, J.G. Morfin et al., "Interpretation of the Nucleon Structure Functions Measured in the Gargamelle SPS Neutrino/Antineutrino Experiment", to be published.

19. Amsterdam-Bologna-Padova-Pisa-Saclay-Torino Collaboration, D. Allasia et al., "Measurement of the Ratios of $\bar{\nu}_{\mu n}$ to $\bar{\nu}_{\mu p}$ Charged Current Cross Sections at High Energies", paper No. 148, submitted to this conference.

20. Jonker, M. et al., Report CERN-EP/81-135 (1981).

21. A recent data set has been presented in Ref. 2.

22. Caltech-Fermilab-Rochester-Rockefeller Collaboration, R. Blair et al., "Recent Results from the CFRR Experiments at Fermilab", contribution to the ν 81 International Conference on Neutrino Physics and Astrophysics, Wailea (1981), presented by M. Shaevitz.

23. Aubert, J.J. et al., Phys. Lett. 105 B (1981) 315;
Aubert, J.J. et al., Phys. Lett. 105 B (1981) 322.

24. Bologna-CERN-Dubna-Munich-Saclay Collaboration, D. Bollini et al., Phys. Lett. 104 B (1981) 403, and A. Argento et al., contribution to the International Conference on High Energy Physics, Lisbon (1981), presented by J. Feltesse.

25. Smatja, G., "μN: Determination of Nucleon Structure Functions", Proceedings of this conference.

26. Kendall, H.W., Proceedings of the 1971 International Symposium on Electron and Photon Interactions at High Energies, Cornell University, p. 247.

27. Aubert, J.J. et al., to be published.

28. Allen, P. et al., Phys. Lett. 103 B (1981) 71.

29. Field, R.D. and R.P. Feynman, Phys. Rev. D 15 (1977) 2590.

30. Glück, M., E. Hoffmann, and E. Reya, Report DO-TH 80/13 (1980).

31. Donnachie, A., and P.V. Landshoff, Phys. Lett. 95 B (1980), 437; see also F.E. Close and R.G. Roberts, Z. Phys. C - Particles and Fields 8 (1981) 57.

32. Hanlon, J. et al., Phys. Rev. Lett. 45 (1980) 1817.

33. Farrar, G.R., P. Schreiner, and W.G. Scott, Phys. Lett. 69 B (1977) 112.

34. Eisele, F., Report DO-EXP 6/81 and Proceedings of the IV Symposium on Elementary Particle Physics, Kazimierz (1981).

35. Abbott, L.F. and R.M. Barnett, Ann. Phys. 125 (1980) 276.

36. Glück, M. and E. Reya, Phys. Lett. 79 B (1978) 453, and Phys. Lett. 83 B (1979) 98.

37. Leveille, J.P., and T. Weiler, Nucl. Phys. B 147 (1979) 147.

38. Aubert, J.J. et al., Phys. Lett. 94 B (1980) 96, and Phys. Lett. 94 B (1980) 101.

39. Clark, A.R. et al., Phys. Rev. Lett. 45 (1980) 1465.

40. Brodsky, S.J., P. Hoyer, C. Peterson, and N. Sakai, Phys. Lett. 93 B (1980) 451; S.J. Brodsky, C. Peterson, and N. Sakai, SLAC-PUB-2660 (1981).

41. Aubert, J.J. et al., "An Experimental Limit on the Intrinsic Charm Component of the Nucleon", to be published.

42. For a recent review on perturbative QCD see A.J. Buras, Physica Scripta 23 (1981) 863.

43. Bardeen, W.A., A.J. Buras, D.W. Duke, and T. Muta, Phys. Rev. D 18 (1978) 3998.

44. Nachtmann, O., Nucl. Phys. B 63 (1973) 237, and Nucl. Phys. B 78 (1974) 455.

45. Gonzàles-Arroyo, A.,C. López, and F.J. Yndurâin, Nucl. Phys. B 153 (1979) 161, and Nucl. Phys. B 159 (1979) 512.

46. Bialas, A., and A.J. Buras, Phys. Rev. D 21 (1980) 1825.

47. Gross, D.J., and C.H. Llewellyn Smith, Nucl. Phys. B 14 (1969) 337.

48. Isaev, P.S., Yu.P. Ivanov, S.G. Kovalenko, and I.S. Zlatev, "Approximated Solution of QCD Evolution Equations", paper No. 67; submitted to this conference.

49. Barbieri, R., J. Ellis, M.K. Gaillard, and G.G. Ross, Nucl. Phys. B 117 (1976) 50.

50. Georgi, H., and H.D. Politzer, Phys. Rev. D 14 (1976) 1829.

51. For a discussion of higher twist contributions see e.g. Ref. 42.

52. Pennington, M.R., F. Megahed, and E.J. Squires, "A Bag-Like Model for Kinematic Corrections to Structure Functions", University of Durham Report, January 1981.

53. Buras, A.J., and K.J.F. Gaemers, Nucl. Phys. B 132 (1978) 249.

54. Aubert, J.J. et al., Z. Phys. C - Particles and Fields 10 (1981) 101.

55. Anderson, H.L., H.S. Matis, and L.C. Myrianthopoulos, Phys. Rev. Lett. 40 (1978) 1061.

56. Bosetti, P.C. et al., Nucl. Phys. B 142 (1978) 1.

57. de Groot, J.G.H. et al., Phys. Lett. 82 B (1979) 292, and Phys. Lett. 82 B (1979) 456.

58. Ball, R.C. et al., Report MSU-CSL-80.

59. Leenen, M., private communication.

Discussion

D.P. Roy, T.I.F.R. Bombay: Since the intrinsic charm prediction is only an asymptotic prediction it should be compared with data only for W^2 well above the threshold (about 200 GeV^2). Doing so one sees that all the EMC data points shown here are consistent with 1 % intrinsic charm, except for the last one ($x = .42$) which does not go beyond $W^2 \sim 80\ GeV^2$, and hence cannot be meaningfully compared.

J. Drees: As you pointed out already the W^2 of this point is of order 80 GeV^2 and thus certainly some distance above threshold. Furthermore, one has to consider the fact that the photon gluon fusion process is responsible for at least some contribution to F_2^c even at larger x. In Fig. 13 we compared our data with the published theoretical predictions of Brodsky, Hoyer, Peterson and Sakai.

U. Amaldi, CERN: I understand that the CDHS data are not corrected for Fermi motion. Which will be the variations in the quoted Λ value of the CDHS collaboration if this correction were included?

J. Drees: I would like to pass on this question to somebody from the CDHS collaboration. For the EMC iron data we also studied the change of the value of Λ originating from an inclusion of Fermi motion corrections. Quoting the effect in terms of the percentage change, we find an increase $\Delta\Lambda/\Lambda = +25$ % which is somewhat less than the percentage change found by the CHARM collaboration but is pointing in the same direction.

H. Wahl, CERN: We tried to make that correction and agree that Λ would increase. However, the bad point is the theoretical uncertainty.

U. Amaldi: Still I would think that this correction should be applied at least to first order before combining the result with the output of other experiments.

G. Wolf, DESY: A question to the charm piece of F_2: In Fig. 12 F_2^c was plotted versus Q^2 for fixed x. What happens if F_2^c is plotted versus Q^2 for fixed W?

J. Drees: If one plots the charmed piece of F_2 at a given fixed x versus W^2 one obtains again the curves shown in the figure.

R. Taylor, SLAC: What is the effect of SLAC-MIT/EMC normalization differences, or R differences, on the higher twist analysis?

J. Drees: The problem when comparing F_2 data sets is twofold: First, one has to be very careful to compare only data which are exactly in the same kinematical region. Second, one has to assume one value of R. If we compare the EMC hydrogen data with the SLAC hydrogen data and restrict ourselves to the kinematical region where our 120 GeV data overlap with the SLAC data we find a ratio SLAC/EMC = .99

assuming $R = 0$ both for SLAC and our data. Assuming $R = .21$ for the SLAC data and $R = 0$ for our data we find a ratio of 1.11. However, let me emphasize that neither the EMC nor the SLAC group really measures R in the region where the data overlap. At each fixed x SLAC measures at smaller values of Q^2 than the EMC. Maybe the best would be to compare the data by assuming a constant value of R somewhere in the middle between 0 and 0.21. Anyway, my personal conclusion from these studies is that the agreement between the data is very good. With respect to the higher twist analysis we made the following check which is independent of any assumption about R for the SLAC data: We repeated the fitting procedure using the separated F_2 values from SLAC-MIT together with the EMC hydrogen data ($R = 0$). The results obtained for the twist 4 contribution remain practically unchanged.

E.L. Berger, Argonne Nat. Lab.: This is a comment on the functional form in x of your twist 4 contribution. You find that $h_4(x)$ varies as $(1-x)^{-2}$, exactly as specified by Blankenbecler, myself, and others at SLAC a few years ago. The physical explanation for two powers of $(1-x)$ is quite simple: We imagine that the high twist effect is due to scattering from integer spin substructure in the nucleon, such as a diquark. If so, then helicity constraints specify two powers of $(1-x)$ difference between the leading twist.

J. Drees: We are quite aware of the fact that this functional form is close to what is expected for a diquark model.

R.L. Jaffe, MIT: I have two comments on the presentation of higher twist structure functions extracted from these data: First, target mass corrections are large and well understood. They should be incorporated in the twist 2 analysis by using Nachtmann moments or the Nachtmann ξ variable. Otherwise they will be likely to obscure true twist 4 effects. Second, the operator product expansion shows that the twist 4 structure function is conceptually independent of the twist 2 structure function. It would be better to attempt functions of the form

$$F(x,Q^2) = F_2(x,Q^2) + h_4(x)/Q^2$$

rather than

$$F(x,Q^2) = F_2(x,Q^2)(1 + h_4(x)/Q^2).$$

J. Drees: Thank you for this comment. Maybe I can add that we intend to perform an analysis of a similar type with the target mass correction formalism being included. One can then immediately see the difference of the higher twist contributions in the two cases.

M. Moshe, Technion Haifa: Indeed, as it has been shown here, high twists are probably important at $x = 1$. However, one should notice as well that as $x \to 1$ also the higher order corrections in the twist 2 series grow fast (this growth still exists even when the most leading terms are resumed, see e.g. Phys. Lett. 98B,

297 (1981)). In general, one should therefore be cautious when analyzing the data with respect to twist 2 plus higher twist terms and avoid the regime close to $x = 1$ where the twist 2 perturbation expansion starts to be questionable.

J. Drees: If one includes these higher order corrections for the case of fits to the EMC data alone then one finds that the corrections are very small in the x region covered, i.e. $x \leq 0.65$.